



Efficient catalytic conversion of glucose into 5-hydroxymethylfurfural by aluminum oxide in ionic liquid

Qidong Hou, Meinan Zhen, Weizun Li, Le Liu, Jinpeng Liu, Shiqiu Zhang, Yifan Nie, Chuanyunlong Bai, Xinyu Bai, Meiting Ju*

Tianjin Engineering Research Center of Biomass Solid Waste Resources Technology, College of Environmental Science and Engineering, Nankai University, Tianjin, 300350, PR China



ARTICLE INFO

Keywords:
5-hydroxymethylfurfural
Glucose
Heterogeneous catalysis
Dehydration
Ionic liquid

ABSTRACT

Conversion of biomass-derived glucose to 5-hydroxymethylfurfural (HMF) is an important step for valorizing lignocellulosic biomass. In conventional reaction systems such as aqueous or water-organic solvent biphasic system, degradation of the formed HMF and other intermediates into undesired products is inevitable due to the presence of Brønsted acid, limiting HMF production efficiency. Here, we develop a novel reaction system consisting of heterogeneous catalyst with reduced Brønsted acidity and ionic liquid 1-ethyl-3-methylimidazolium bromide (EMIMBr) to achieve the efficient conversion of high-concentration glucose to HMF. A series of Al-containing materials was synthesized and characterized by N_2 adsorption-desorption, XRD, XPS, FTIR, Py-IR and CO_2 TPD, among which the Al_2O_3 -b-0.05 prepared by simple alkaline treatment exhibited high Lewis acidity and low Brønsted acidity. The Al_2O_3 -b-0.05 in the medium of EMIMBr led to the highest HMF yield of 49.7% from high-concentration glucose (up to 10 wt%), as is more efficient than the heterogeneous EMIMCl/ Al_2O_3 -b-0.05 and homogeneous EMIMBr/ $AlCl_3$ system. This work provides a paradigm of improving HMF production efficiency via the combined use of heterogeneous Lewis acid catalyst and ionic liquid.

1. Introduction

The utilization of renewable lignocellulosic biomass with an estimated annual production about 2×10^{11} metric tons to produce alternative biofuels, fine chemical and materials is a promising approach to replace fossil resources with reduced emission of carbon dioxide [1]. The most abundant component (approximately 75%) in biomass are carbohydrates, including cellulose and hemicellulose which are produced from carbon dioxide and water through photosynthesis [2,3]. Cellulose is composed of D-glucose units linked via β -1,4-glycosidic bonds, while hemicellulose is a heteropolymer mainly composed of xylose units with a few other sugars, including mannose, galactose, rhamnose, and arabinose [4–6]. Several platform chemicals, especially 5-hydroxymethylfurfural (HMF) and furfural can be produced from glucose and xylose via acid catalytic processes [7,8]. As one of the most important platform chemicals, HMF can be used as a starting material for the production of a series of value-added products [9,10]. For example, it is very attractive to use HMF-derived compound furan-2,5-dicarboxylic acid (FDCA) to react with sugar-derived ethylene glycol to synthesize fully biomass-based polyethylene furandicarboxylate (PEF),

which may potentially replace petroleum-derived polyethylene terephthalate (PET) [11,12]. However, the cost of HMF is 3 orders of magnitude higher than that of currently used bulk chemicals derived from fossil resources, strongly limiting its large scale production and commercial application.

Numerous efforts have been devoted to the conversion of C_6 monosaccharides into HMF. The dehydration of fructose into HMF is easy to achieve with high efficiency, but the cost of HMF is still high due to the low abundance of fructose in the nature [13–17]. Compared with fructose, glucose is readily available and generally considered as cheap feedstock. Nevertheless, the conversion of glucose to HMF is much more challenging than the conversion of fructose due to the high activation energies ($36.4 \text{ kcal mol}^{-1}$) of direct glucose dehydration [18]. In the aqueous solution, the HMF yield is usually low due to the severe degradation of HMF. The biphasic reaction systems consisting of water and organic solvents, which could transfer the formed HMF from water phase to the organic phase instantaneously, were used extensively to reduce further degradation of HMF in the reaction phase [19]. In such biphasic reaction systems, NaCl was widely employed to enhance the transfer of HMF from reaction phase to the extract phase.

* Corresponding authors.

E-mail address: jumeit@nankai.edu.cn (M. Ju).

The use of organic solvents such as dimethyl sulfoxide (DMSO), tetrahydrofuran (THF) and γ -valerolactone (GVL) as co-solvent, were also demonstrated to be effective to inhibit the HMF degradation catalyzed by Brønsted acid in aqueous solution [20–22]. Although some metal chlorides, metal oxides, metal phosphates, mineral acids, zeolite as well as their combinations have been demonstrated to be active for the conversion of glucose in water-organic solvent biphasic reaction systems, the intrinsic HMF production efficiencies of these reaction systems are low in view of the harsh reaction conditions, the low concentration of glucose (usually lower than 3 wt% with respect to the solvent), the high loading of catalyst as well as the use of large amount of organic solvents and salts [1,18,23,24].

The combination of certain ionic liquids and homogenous metal chlorides, such as EMIMCl/CrCl₂, BMIMCl/CrCl₃ and EMIMBr/SnCl₄ could convert high concentration glucose (10 wt% with respect to the solvent) to HMF with high HMF yield and selectivity, but the instability and toxicity of these metal chlorides seriously impedes their actual application [25,26]. Exploitation of highly active and cost-effective heterogeneous catalysts and catalytic processes with high efficiency hold the key to achieve the large-scale production and commercial application of HMF. Recently, we found that tin phosphate (SnPO) can be used as a heterogeneous catalyst for the efficient dehydration of high concentration glucose into HMF in ionic liquid EMIMBr. Since EMIMBr could convert fructose into HMF almost quantitatively in the absence of any other catalysts, the use of EMIMBr as reaction medium could shift the equilibrium of glucose isomerization into fructose. The HMF production efficiency from glucose in the SnPO/EMIMBr system was significantly improved owing to the synergistic effect between SnPO and EMIMBr. However, the synthesis of SnPO catalyst require complex and energy-consuming processes. Recently, Al-containing materials, including Al₂O₃, Zeolites and their amorphous SiO₂–Al₂O₃ counterparts have been widely used in a variety of industrial catalytic processes as well as biorefinery processes, owing to their relative low cost, high specific surface area and tuned Lewis and Brønsted acid sites [27–29]. The screening of Al-containing materials should open opportunities of innovation for cost-effective heterogeneous catalysts which are suitable for HMF production.

In this work, we propose an alternative approach that uses heterogeneous catalyst with high Lewis acidity and low Brønsted acidity to convert glucose to HMF in the medium of ionic liquid EMIMBr. A series of Al-containing materials were prepared and tested as heterogeneous catalysts for the dehydration of glucose into HMF in ionic liquid. The influences of temperature, time and solvent on HMF yields were investigated to optimize the reaction conditions for HMF production. The role of catalyst and ionic liquid was illustrated via characterization of the catalyst and control experiments.

2. Experiment

2.1. Materials and reagents

Fructose (99%), glucose (99%), 5-hydroxymethylfurfural (99%), AlCl₃·6H₂O, and dimethyl formamide (DMF, 99%) were purchased from Tianjin Heowns Biochem LLC (Tianjin, China). Ionic liquids EMIMCl (99%) and EMIMBr (99%) were purchased from Shanghai Chengjie Chemical Reagent Co. Ltd., China. All the other chemical reagents were purchased from commercial sources in China and used as received. Commercial neutral aluminum oxide (200–300 meshes, AR), which have been denoted as Al₂O₃-n, was purchased from Tianjin Kemiou Chemical Reagent Co., Ltd.

2.2. Material synthesis

Al₂O₃-n was employed as starting materials for the preparation of acid and basic aluminum oxide. Alkaline and acid treatments were performed by immersing 4.0 g of Al₂O₃-n in 100 mL of 0.05 M NaOH,

0.2 M NaOH [30] and 0.27 M HCl solution, respectively, at room temperature for 24 h under vigorous stirring. The treated solid was collected by centrifugation at 10,000 rpm for 30 min and then washed with water and ethanol five times, respectively, to remove the soluble substance and free ions. Subsequently, the solid was dried at 80 °C for 24 h, finely grinded and calcined at 700 °C for 5 h. The Al₂O₃ treated with 0.05 M NaOH, 0.2 M NaOH and 0.27 M HCl solution are abbreviated as Al₂O₃-b-0.05, Al₂O₃-b-0.20 and Al₂O₃-a, respectively.

Aluminum phosphate was prepared according to our previously described method [24]. Briefly, 2 g of templating agent P123, 2.30 g of H₃PO₄ (20 mmol) were dissolved in 30 mL of H₂O. 4.83 g of AlCl₃·6H₂O (20 mmol) was dissolved in 10 mL of H₂O. The AlCl₃ solution was added to the H₃PO₄ solution gradually under stirring to obtain a synthesis mixture. The synthesis mixture was transferred into a polypropylene bottle and aged at 100 °C for 72 h. After aging, the obtained colloidal precipitate was collected by filtration, followed by washing and drying at 80 °C for 24 h. Finally, the material was calcined at 700 °C for 5 h and this calcined sample was denoted as AlPO.

2.3. Catalyst characterization

The crystal phases in catalyst samples were investigated by using wide-angle XRD analysis on a X'pert MFD diffractometer with Cu-K α radiation ($\lambda = 1.5406 \text{ \AA}$) generated at a voltage of 40 kV and a current of 40 mA. X-ray photoelectron spectra (XPS) was carried out using an ESCALAB 250Xi X-ray Photoelectron Spectrometer (Thermo Fisher Scientific, America). Peak positions were calibrated according to the spurious C1s signal at 284.6 eV binding energy. The N₂ isothermal adsorption/desorption was recorded at 77 K on an automatic ASAP 2460 system from Micromeritic. The FTIR spectra were obtained on an FTS 6000 FTIR spectrometer (Bio-rad, USA). ²⁷Al magic angle spinning nuclear magnetic resonance (MAS NMR) spectra were collected using a JEOL 600 MHz NMR spectrometer with a 14.1 T magnet (JNM-ECZ600R, Japan) using a 3.2 mm probe with a spinning frequency of 15 kHz at resonance frequencies of 156 MHz. The amount of CO₂ and NH₃ chemisorbed on each catalyst were measured on a Micromeritics 2920 equipment by CO₂ and NH₃ temperature-programmed desorption (TPD), respectively. Prior to the adsorption of CO₂ and NH₃, the catalyst was degassed in He stream (20 mL min⁻¹) at 550 °C for 2 h. For the determination of CO₂-TPD, the catalyst was cooled to 50 °C and then saturated with a flow of 3% v/v CO₂/He (15 mL min⁻¹) for 1 h. Subsequently, the sample was heated in a pure Ar stream (15 mL min⁻¹) at 50 °C for 50 min to remove any physical adsorbed molecules. The chemisorbed CO₂ is desorbed by heating from 25 °C to 1000 °C at a heating rate of 10 °C min⁻¹. The variation of carbon dioxide concentration in the effluent He stream was determined by a thermal conductivity detector (TCD). For the determination of NH₃-TPD, the catalyst was treated with 7% v/v NH₃/He flow for 15 min and then degassed in pure Ar stream (15 mL min⁻¹) at 50 °C for 40 min. To probe the surface acid sites, pyridine-probed Fourier transformed infrared (Py-IR) spectroscopy was executed on a Bruker TENSOR 27 spectrometer by averaging 64 scans at resolution of 2 cm⁻¹ in the 4000–400 cm⁻¹ range. The detailed testing procedure can be found in our previous report [24].

2.4. Catalytic tests

To investigate the catalytic performance of different catalysts, a mixture of glucose (100 mg), catalyst (50 mg of heterogeneous catalyst, or 0.056 mmol AlCl₃·6H₂O) and solvent (1000 mg of ionic liquid) were loaded to a 10 mL closed thick-walled glass reactor. The reactor was sealed and placed in the oil bath which was preheated to the designed reaction temperature with sufficiently magnetically stirring. After the reaction, the reaction mixture was cooled to room temperature by cold-water bath. The sample was diluted with water and filtered with a 0.45 μm polytetrafluoroethylene filter membrane to remove insoluble

solid, prior to the determination. All reaction products were analyzed by High performance liquid chromatography (HPLC) and quantified using calibration curves. The concentration of HMF was determined at 284 nm and 35 °C by HPLC system equipped with a diode array detector (DAD) using a methanol/water (v: v = 70%: 30%) mobile phase at a flow rate of 1.0 mL/min. The concentration of glucose was analyzed by HPLC system equipped with a refractive index detector (refractomax 521 Model) and a Shodex Sugar SH1011 analytical column (8.0 mm × 300 mmL). A 5 mM H₂SO₄ solution was used as mobile phase at a flow rate of 1.0 mL/min at 65 °C. The calculation of glucose conversion, HMF yield and selectivity was detailed in our previous report [24]. To compare with other catalytic systems, the TOF values of different catalysts at their optimized reaction conditions were calculated at the initial 20 min. For Al₂O₃-n, Al₂O₃-a, Al₂O₃-b-0.05, Al₂O₃-b-0.20 and AlPO, the reaction was performed at 140 °C using a catalyst loading of 0.05 g and glucose loading of 0.10 g. For AlCl₃, the reaction was performed at 80 °C using a catalyst loading of 0.0134 g (AlCl₃/glucose molar ratio = 10%) and glucose loading of 0.10 g. The glucose conversion was no more than 25% to ensure the accuracy of the calculated TOF values. HMF formation rate (h⁻¹) and glucose conversion rate (h⁻¹) were calculated using the following formula:

$$\text{HMF formation rate} = \frac{\text{moles of formed HMF}}{\text{time} * \text{moles of Al}^{3+} \text{ in the catalyst}} \quad (1)$$

$$\text{Glucose conversion rate} = \frac{\text{moles of reacted glucose}}{\text{time} * \text{moles of Al}^{3+} \text{ in the catalyst}} \quad (2)$$

The catalytic tests were replicated at least three times, and the reproducibility of glucose conversion, HMF yield and HMF selectivity were within 3% standard deviation.

3. Results and discussion

3.1. Catalyst characterization

3.1.1. Morphology and structure

N₂ adsorption-desorption isotherms were determined to examine the specific surface area and pore size distribution of Al₂O₃-n, Al₂O₃-a, Al₂O₃-b-0.05, Al₂O₃-b-0.20 and AlPO. As shown in Fig. 1a, the isotherms of Al₂O₃-n, Al₂O₃-a, Al₂O₃-b-0.05 and Al₂O₃-b-0.20 were classic IV type curves with apparent H4 hysteresis loops (IUPAC), corresponding to the typical feature of mixed microporous and mesoporous structure. Their pore size distributions are exhibited in Fig. 1b. The BET specific surface area (S_{BET}), pore volume (V_{pore}), and average pore size (D_{meso}) of these catalysts was calculated according to the nitrogen adsorption-desorption isotherms and summarized in Table 1. After acid treatment, the specific surface area of Al₂O₃ decreased from 138.7–102.7 m² g⁻¹, the pore volume increased from 0.21 to 0.26 cm³ g⁻¹ and the average pore size increased from 1.7–3.1 nm. The alkaline treatments in 0.05 and 0.20 M NaOH solution both led to the increase of pore volume and average pore size as well as the slight decrease of specific surface area, compared with the neutral aluminum oxide. The specific surface area, pore volume and average pore size of Al₂O₃-b-0.20 were slightly larger than that of Al₂O₃-b-0.05. In contrast, the isotherm of AlPO is typical IV type curves with H3 hysteresis loop which is different from that of Al₂O₃ samples. Compared with the four Al₂O₃ samples, AlPO exhibited remarkably larger specific surface area, pore volume and average pore size.

The crystal structures of Al₂O₃-n, Al₂O₃-a, Al₂O₃-b-0.05, Al₂O₃-b-0.20 and AlPO were investigated by XRD. As shown in Fig. S1, the XRD patterns of Al₂O₃-n, Al₂O₃-a, Al₂O₃-b-0.05 and Al₂O₃-b-0.20 samples were in good agreement with JCPDS 29-0063, indicating that these samples are typical γ -Al₂O₃ [31]. The predominant characteristic diffraction peaks at 37.59, 45.80 and 67.10°, as well as the weak diffraction peaks at 19.44 and 39.47° were well indexed to the lattice planes of (311), (400), (440), (111) and (222) of γ -Al₂O₃, respectively

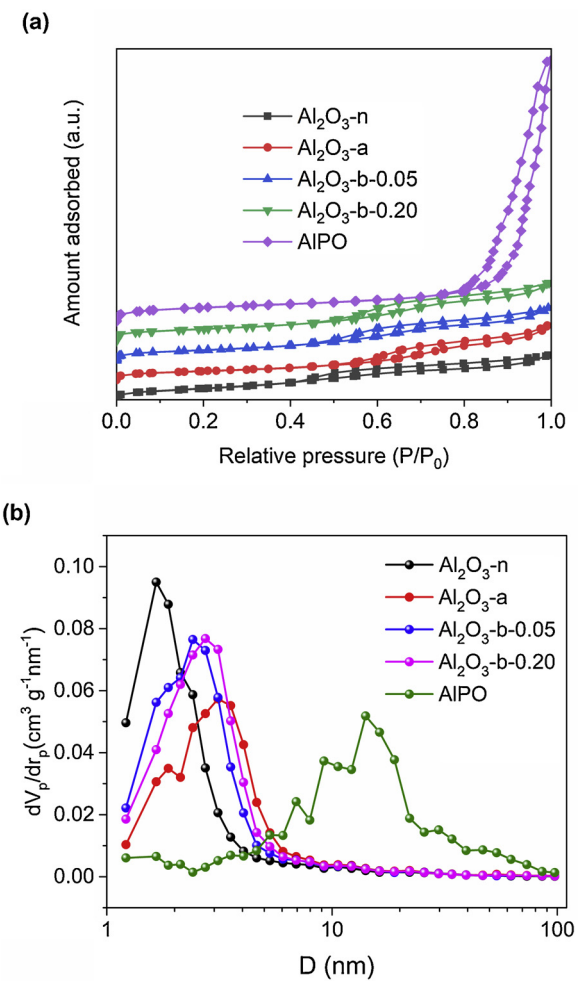


Fig. 1. (a) N₂ adsorption-desorption isotherms and (b) pore size distributions curves of Al₂O₃-n, Al₂O₃-a, Al₂O₃-b-0.05, Al₂O₃-b-0.20 and AlPO.

Table 1

Properties of the synthesized Al₂O₃-n, Al₂O₃-a, Al₂O₃-b-0.05, Al₂O₃-b-0.20 and AlPO.

Catalyst	Al ₂ O ₃ -n	Al ₂ O ₃ -a	Al ₂ O ₃ -b-0.05	Al ₂ O ₃ -b-0.20	AlPO
S _{BET} (m ² g ⁻¹)	138.7	102.7	125.5	135.3	162.1
V _{pore} (cm ³ g ⁻¹)	0.21	0.26	0.25	0.27	1.14
D _{meso} (nm)	1.7	3.1	2.4	2.7	14.1
Al/O atomic ratio	0.564	0.615	0.603	0.613	
Fraction of AlO ₄	0.465	0.472	0.344	0.433	
A _{CO2} (μmol CO ₂ g ⁻¹)	4.5	4.9	5.3	5.8	164.0

[32,33]. The XRD patterns of these Al₂O₃ catalysts did not have noticeable difference, suggesting that the alkaline and acid treatments at ambient temperature didn't change the crystal structures of Al₂O₃. The characteristic diffraction peaks at 18.28 and 20.28° attributed to sodium aluminum oxide (Al₂Na₂O₄), which was formed after loading 7.6 wt% Na₂O onto the commercial Al₂O₃ SCFa [31,34], was not obvious in the Al₂O₃-b-0.05 and Al₂O₃-b-0.20 samples, demonstrating that the Al₂Na₂O₄ content in the present Al₂O₃ samples is under the detection limit of XRD. As expected, AlPO showed a very broad hump in the range of 15–26°, which is the typical XRD patterns for an amorphous material [35,36].

3.1.2. Surface chemical state

The FTIR spectra of Al₂O₃-n, Al₂O₃-a, Al₂O₃-b-0.05, Al₂O₃-b-0.20 and AlPO are showed in Fig. S2. The FTIR spectra of Al₂O₃-n, Al₂O₃-a,

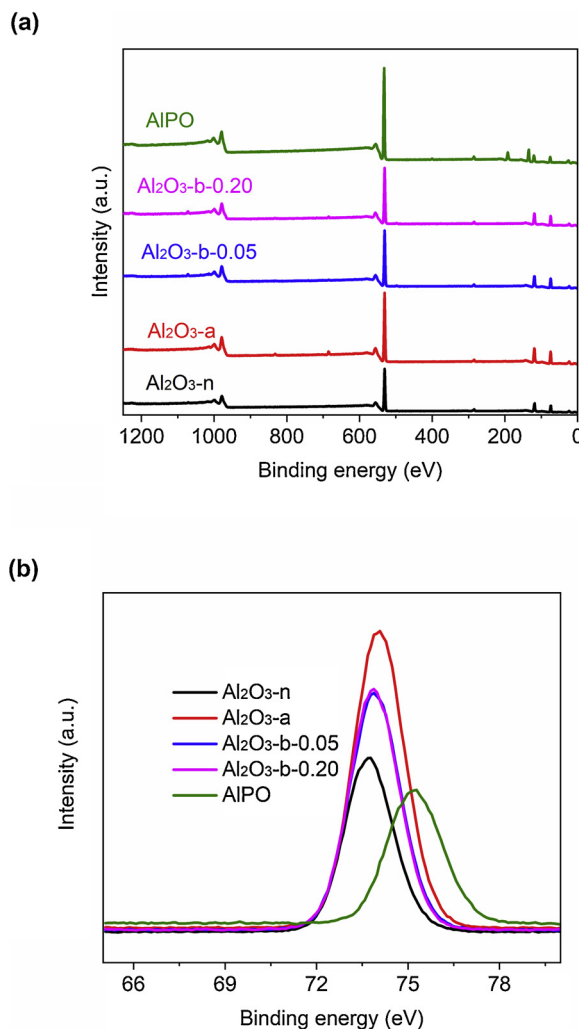


Fig. 2. Wide XPS spectra (a) and high-resolution Al 2p XPS spectra (b) of Al_2O_3 -n, Al_2O_3 -a, Al_2O_3 -b-0.05, Al_2O_3 -b-0.20 and AlPO.

Al_2O_3 -b-0.05 and Al_2O_3 -b-0.20 exhibited same bands at around 841, 593, 494 and 457 cm^{-1} . The FTIR spectra of AlPO exhibited a broad band in the range of $1000\text{--}1200\text{ cm}^{-1}$ which can be attributed to the O–P–O asymmetric stretching vibrations, confirming the existence of phosphate or polyphosphate species in AlPO [35,37]. The band at 1300 cm^{-1} attributed to P–OH deformation was absent in the AlPO [37] and the band at around 3400 cm^{-1} corresponded to OH [36] was weak in all the samples, confirming the content of OH is low in these catalysts.

The XPS spectra of Al_2O_3 -n, Al_2O_3 -a, Al_2O_3 -b-0.05, Al_2O_3 -b-0.20 and AlPO were measured to analyze the surface chemistry of these catalysts. The weak peak at 685.1 and 833.0 eV which are attributed to F, instead of Cl element, appeared in the XPS spectra of Al_2O_3 -a (Fig. 2a). It was inferred that the F element is resulted from the F[–] impurity from the concentrated hydrochloric acid since Al_2O_3 have been demonstrated to be very capable to adsorb fluoride [38,39]. The weak peak at around 1071.2 eV in the XPS spectra of Al_2O_3 -b-0.05 and Al_2O_3 -b-0.20 was corresponded to Na element, suggesting that small amount of Na is introduced onto the Al_2O_3 surface during the alkaline treatment process. The high-resolution Al 2p XPS spectra of Al_2O_3 -n, Al_2O_3 -a, Al_2O_3 -b-0.05, Al_2O_3 -b-0.20 and AlPO (Fig. 2b) exhibited the Al 2p characteristic peak at 73.7, 73.9, 74.0, 74.0 and 75.2 eV , respectively. Moreover, the Al/O atomic ratio increased in the following order: Al_2O_3 -n < Al_2O_3 -b-0.05 < Al_2O_3 -b-0.20 < Al_2O_3 -a, confirming that the alkaline and acid treatments could influence the element

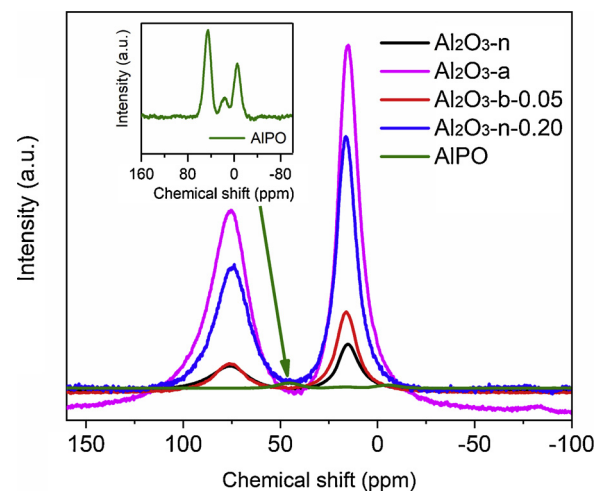


Fig. 3. ^{27}Al MAS NMR spectra of Al_2O_3 -n, Al_2O_3 -a, Al_2O_3 -b-0.05, Al_2O_3 -b-0.20 and AlPO.

content in the surface of catalysts (Table 1).

The high-resolution solid-state ^{27}Al MAS NMR spectra of Al_2O_3 -n, Al_2O_3 -a, Al_2O_3 -b-0.05, Al_2O_3 -b-0.20 and AlPO were measured to probe coordination environment of aluminum atoms. Two prominent peaks at 15 and 76 ppm present in the ^{27}Al MAS NMR spectra (Fig. 3) of Al_2O_3 -n, Al_2O_3 -a, Al_2O_3 -b-0.05 and Al_2O_3 -b-0.20 were assigned as octahedrally (AlO_6) and tetrahedrally (AlO_4) coordinated Al^{3+} species, respectively [40]. The characteristic peak of unsaturated pentacoordinate Al^{3+} species (AlO_5 at 38 ppm) was very weak in these materials [41]. The intensity of the peaks corresponded to tetrahedrally and octahedrally coordinated Al^{3+} sites present on the surface of Al_2O_3 -a and Al_2O_3 -b-0.20 increased remarkably, compared with Al_2O_3 -n [42]. The intensity of peak corresponded to octahedrally coordinated Al^{3+} sites present on the surface of Al_2O_3 -b-0.05 was obviously higher than that of Al_2O_3 -n, but the intensity of peak corresponded to tetrahedrally coordinated Al^{3+} sites was almost unchanged. The fraction of tetrahedrally coordinated Al species were quantified by integrating the ^{27}Al MAS NMR spectra [30,42]. As shown in Table 1, the fraction of tetrahedrally coordinated Al sites increased slightly after acid treatment. The alkaline treatment in 0.05 M NaOH solution leaded to obvious decrease of the fraction of tetrahedrally coordinated Al sites, while alkaline treatment in 0.20 M NaOH solution resulted in the slight decrease of the fraction of tetrahedrally coordinated Al sites.

3.1.3. Acidity and basicity properties

The amount and strength of the acid sites of the catalysts were analyzed by NH_3 -TPD (Fig. S3). Al_2O_3 -n showed two broad peaks centered at 265 and $600\text{ }^\circ\text{C}$, corresponding to the weak and strong acidic sites, respectively. Al_2O_3 -a, Al_2O_3 -b-0.05 and Al_2O_3 -b-0.20 exhibited one broad peak in the range of $200\text{--}700\text{ }^\circ\text{C}$ with reduced intensity, suggesting that the amount of acidic sites decreased after alkaline and acid treatments. In contrast, AlPO only showed one peak corresponding to the weak acidic sites.

Since acid type (Brønsted versus Lewis acid) has a crucial influence on the conversion of glucose, the amount of Brønsted and Lewis acid sites at different temperature were further determined by FTIR spectra after pyridine chemisorption. Among the tested catalysts, Al_2O_3 -n exhibited the highest Lewis and Brønsted acidity, in agreement with NH_3 -TPD results (Fig. 4a). Previous study has showed that the Lewis acidic sites of $\gamma\text{-Al}_2\text{O}_3$ are stable when exposing to water at $180\text{ }^\circ\text{C}$ for 7 h [43]. As the temperature increased from 100 to $400\text{ }^\circ\text{C}$, the amount of Brønsted and Lewis acid sites decreased from 569.2 and $699.1\text{--}225.9$ and $123.0\text{ }\mu\text{mol g}^{-1}$, respectively, with Brønsted/Lewis acid ratio increasing from 0.81 to 1.84 . At $100\text{ }^\circ\text{C}$, the amount of Brønsted acid sites ($218.0\text{ }\mu\text{mol g}^{-1}$) in Al_2O_3 -a was obviously lower than that in Al_2O_3 -n,

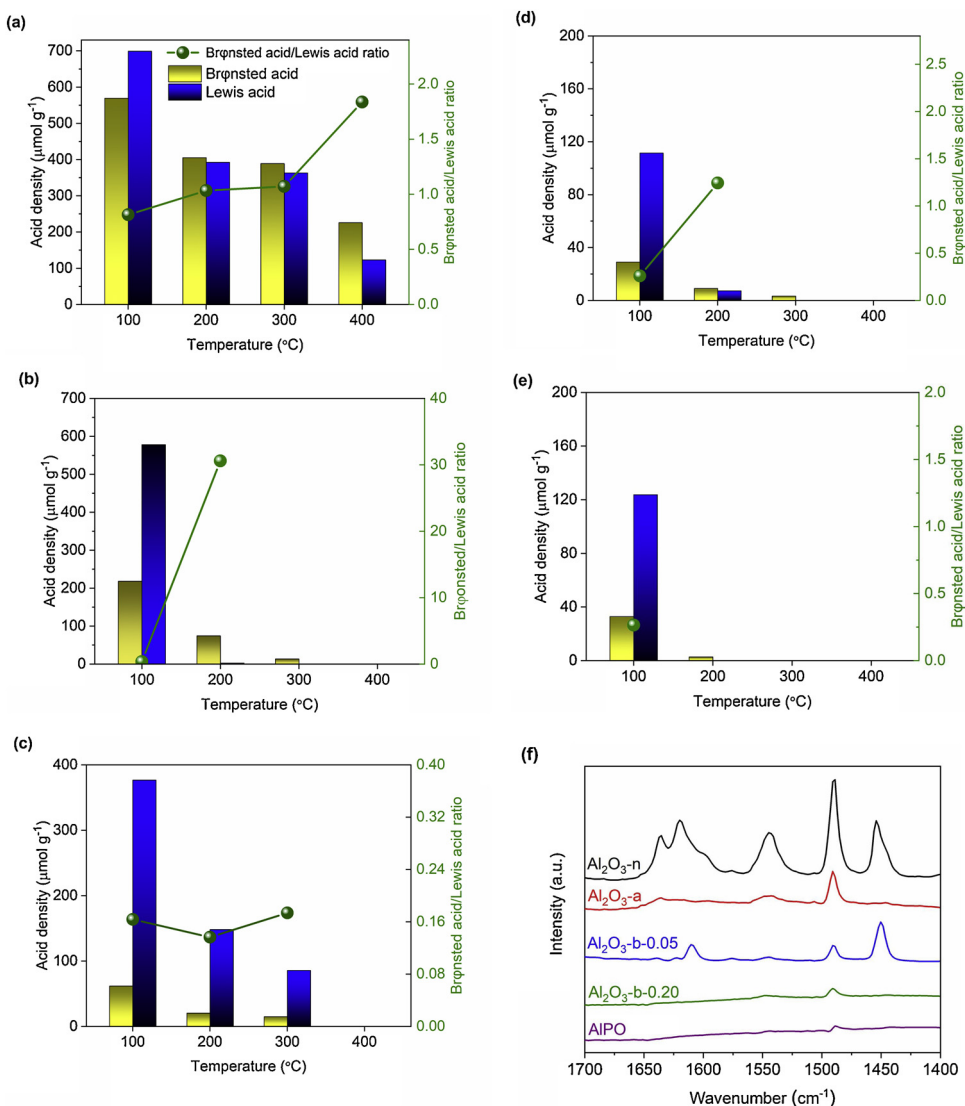


Fig. 4. Acid distribution of (a) Al₂O₃-n, (b) Al₂O₃-a, (c) Al₂O₃-b-0.05, (d) Al₂O₃-b-0.20 and (e) AlPO, and (f) FTIR spectra after pyridine adsorption at 200 °C.

while the amount of Lewis acid sites (578.1 μmol g⁻¹) in the former was slightly lower than the latter. The amount of Brønsted acid sites in Al₂O₃-a decreased quickly with the increase of temperature, while the Lewis acid sites disappeared completely when the temperature was more than 200 °C (Fig. 4b). The amount of Lewis acid sites in Al₂O₃-b-0.05 were remarkably higher than its Brønsted acid sites at the temperature between 100–300 °C, as is different from other catalysts (Fig. 4c). For Al₂O₃-b-0.20 and AlPO, both the amount of Brønsted and Lewis acid sites were low when the temperature was more than 200 °C (Figs. 4d and e). Since the conversion of glucose over these catalysts were usually performed between 100–200 °C, the FTIR spectra after pyridine adsorption at 200 °C were analyzed to confirm their acid distributions (Fig. 4f). The FTIR spectra of Al₂O₃-n and Al₂O₃-b-0.05 after pyridine adsorption showed predominant peaks at 1450 and 1612 cm⁻¹ attributed to vibrations characteristic of pyridine sorption on strong Lewis acid sites (denoted with SL), small peak at 1576 cm⁻¹ attributed to weak Lewis acid sites (WL) and peak at around 1637 cm⁻¹ assigned to the Brønsted acidic sites [70]. The peaks at 1543 cm⁻¹ attributed to Brønsted acidic sites and 1489 cm⁻¹ attributed to the overlap of Brønsted and Lewis acid sites decreased in the following order: Al₂O₃-n > Al₂O₃-a > Al₂O₃-b-0.05 > Al₂O₃-b-0.20 ≥ AlPO [75]. The combined NH₃-TPD, Py-IR and ²⁷Al NMR analysis indicated that the mild alkaline treatment (0.05 M NaOH) is effective to block most Brønsted

acid sites and weak Lewis acid sites, thus leading to the high Lewis acidity and low Brønsted acidity of Al₂O₃-b-0.05, as is consistent with the reduced fraction of tetrahedrally Al³⁺ (Fig. 3) [30].

The CO₂ temperature programmed desorption (CO₂-TPD) curves of Al₂O₃-n, Al₂O₃-a, Al₂O₃-b-0.05, Al₂O₃-b-0.20 and AlPO were measured to analyze their base properties. As shown in Fig. 5, the TPD curves of Al₂O₃-n, Al₂O₃-a, Al₂O₃-b-0.05 and Al₂O₃-b-0.20 exhibited similar weak peak between 100 and 180 °C, which are attributed to the low-strength basic sites. In contrast, the TPD curves of AlPO exhibited strong peak at around 390 °C, which are attributed to the high-strength basic sites. The amount of basic sites (A_{CO2}) was calculated by integrating the deconvoluted peaks from the TPD curves. As shown in Table 1, the total amount of basic sites for Al₂O₃-n, Al₂O₃-a, Al₂O₃-b-0.05 and Al₂O₃-b-0.20 (4.5–5.8 μmol CO₂ g⁻¹) were obviously lower than that of AlPO (164.0 μmol CO₂ g⁻¹).

3.2. Catalytic study

3.2.1. Influence of catalyst on the conversion of glucose to HMF

The catalytic activity of Al₂O₃-n, Al₂O₃-a, Al₂O₃-b-0.05, Al₂O₃-b-0.20 and AlPO were investigated for the conversion of glucose into HMF using ionic liquid EMIMBr as reaction medium. Among the tested catalysts, Al₂O₃-b-0.05 exhibited the highest HMF yield of 34.5% after

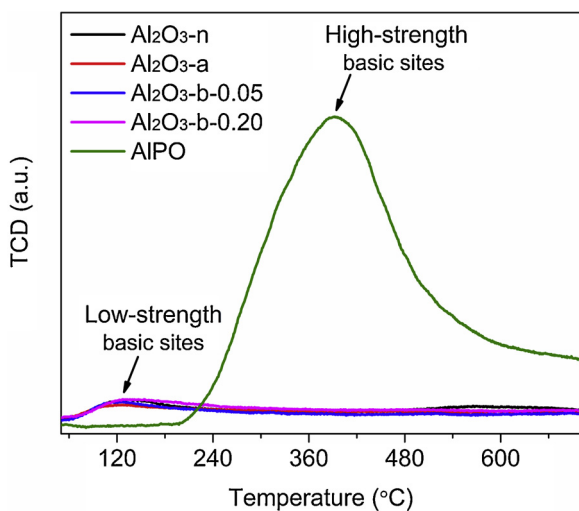


Fig. 5. CO_2 -TPD curves of Al_2O_3 -n, Al_2O_3 -a, Al_2O_3 -b-0.05, Al_2O_3 -b-0.20 and AlPO .

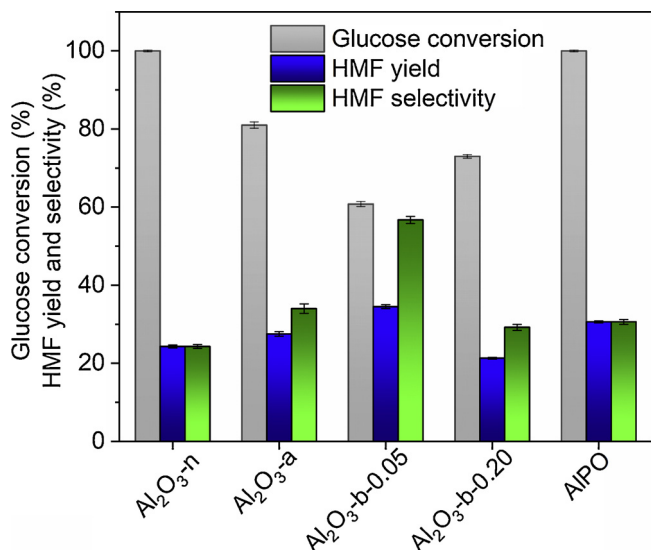


Fig. 6. Influence of catalysts on the dehydration of glucose into HMF in EMIMBr. Conditions: 100 mg of glucose dissolved in 1000 mg of EMIMBr; 50 mg of catalyst; 120 $^{\circ}\text{C}$; 3 h.

3 h reaction at 120 $^{\circ}\text{C}$, with the HMF selectivity as high as 56.7% (Fig. 6). Compared with Al_2O_3 -b-0.05, Al_2O_3 -a and Al_2O_3 -b-0.20 exhibited higher glucose conversion as well as lower HMF yield and selectivity. Although Al_2O_3 -a and AlPO attained high glucose conversion approaching 100%, the HMF yields were only 24.3 and 30.6%, respectively. Since the HMF selectivity obtained with Al_2O_3 -b-0.05 was remarkably higher than the other catalysts, the influence of reaction temperature and time on the catalytic activity of Al_2O_3 -b-0.05 was studied to further improve the HMF yield. As shown in Fig. 7, the HMF yield increased continuously with the reaction time when the conversion of glucose was conducted at 120 $^{\circ}\text{C}$. As the reaction temperature increased to 130 and 140 $^{\circ}\text{C}$, the maximal HMF increased to 48.3 and 49.7% with the reaction time reduced to 4 and 3 h, respectively. To facilitate the comparison of different catalytic systems, the TOF values of different catalysts at their optimized reaction conditions were calculated and summarized in Table 2. The initial glucose conversion rates over different heterogeneous catalysts increased in the following order: Al_2O_3 -n > AlPO \approx Al_2O_3 -a > Al_2O_3 -b-0.20 > Al_2O_3 -b-0.05. In contrast, the initial HMF formation rates over Al_2O_3 -b-0.05 was considerably higher than other tested heterogeneous catalysts, indicating

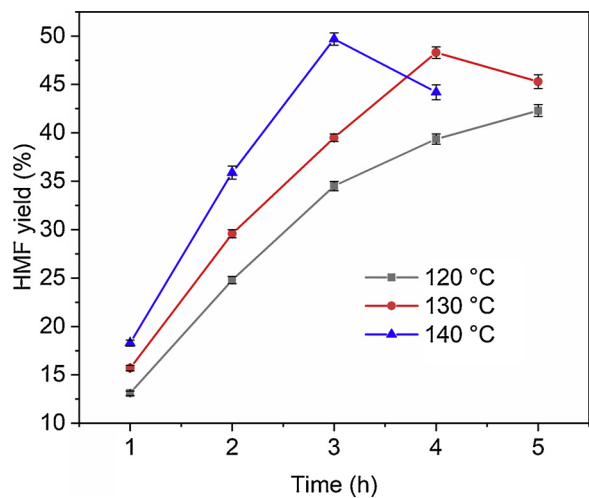


Fig. 7. Influence of temperature and time on dehydration of glucose into HMF in EMIMBr. Conditions: 100 of glucose dissolved in 1000 mg of EMIMBr; 50 mg of Al_2O_3 -b-0.05.

that the high Lewis acidity and low Brønsted acidity are vital for the formation of HMF from glucose conversion.

At the optimized reaction conditions, the recyclability and stability of Al_2O_3 -b-0.05 was evaluated. After reaction, the HMF was extracted from the reaction mixture with 15 ml of glycol dimethyl ether 5 times. For the recycling of catalyst, the reaction mixture was diluted with water. The catalyst was separated through filtration and then washed with water and ethanol 5 times, respectively. The catalyst was dried at 80 $^{\circ}\text{C}$ for 24 h and then calcined at 700 $^{\circ}\text{C}$ for 5 h to remove the possible organic deposits. The regenerated catalyst was reused for glucose conversion. As shown in Fig. 8, the glucose conversion and HMF yield still reached 96.0 and 48.9% after three consecutive catalytic runs, demonstrating the stability and reusability of catalyst under the tested condition.

3.2.2. Influence of solvent on the conversion of glucose to HMF

Recent studies have showed that manipulating the solvent effect is effective to tune the catalytic activity of catalyst, thus remarkably influencing the product yield and selectivity [44–46]. The conversion of glucose to HMF using Al_2O_3 -b-0.05 as catalyst was also conducted in the medium of ionic liquid EMIMCl, one of the most widely employed ionic liquids in biomass conversion. As shown in Fig. 9, both the HMF yield and selectivity obtained with EMIMCl were remarkably lower than that obtained with EMIMBr, suggesting that ionic liquid EMIMBr play an important role in the conversion of glucose to HMF. Recently, we have demonstrated that Br^- containing ionic liquids including EMMBr and BMIMBr could directly convert fructose to HMF in the absence of any other catalysts, which could explain the product difference in these two ionic liquids [26]. We also observed that the combined use of ionic liquid EMMBr with Lewis acids, including homogeneous SnCl_4 and heterogeneous SnPO , could improve the HMF yield remarkably [24]. These works demonstrated that ionic liquid EMIMBr is very important for the improvement of HMF production efficiency.

3.2.3. Influence of AlCl_3 on the conversion of glucose to HMF

As a contrast to the EMIMBr/ Al_2O_3 -b-0.05 heterogeneous system, homogeneous AlCl_3 was investigated for the conversion of glucose to HMF in the medium of ionic liquid EMIMBr. As shown in Fig. S4, when the reaction was conducted at 100 $^{\circ}\text{C}$, the HMF yield didn't exceed 14%. It was observed that the reaction mixture becomes dark rapidly under this condition, suggesting the formation of large amount of humins. As the reaction decreased to 80 $^{\circ}\text{C}$, the highest HMF yield reached 37.3%.

Table 2TOF of different catalysts at their optimized reaction conditions.^a

Catalyst	Al ₂ O ₃ -n	Al ₂ O ₃ -a	Al ₂ O ₃ -b-0.05	Al ₂ O ₃ -b-0.20	AlPO	AlCl ₃
HMF formation rate (h ⁻¹)	0.053	0.062	0.103 (0.052)	0.048	0.056	2.56
Glucose conversion rate (h ⁻¹)	0.276	0.214	0.142 (0.267)	0.199	0.219	5.02

^a Reaction conditions: 100 mg of glucose dissolved in 1000 mg of EMIMBr; 140 °C; 50 mg of catalyst. HMF formation rate and glucose conversion rate were calculated at the initial 20 min. The data in the parentheses represent the TOF values in EMIMCl.

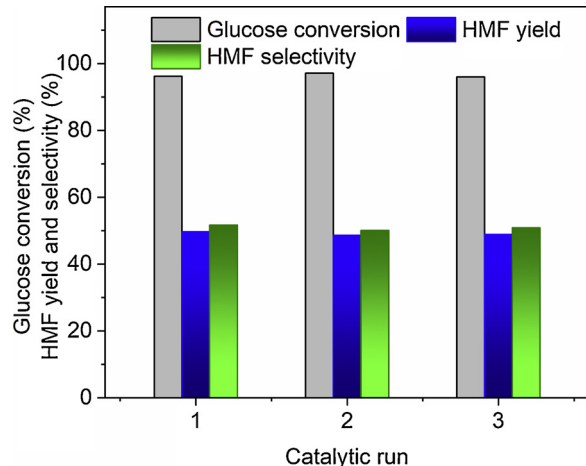


Fig. 8. Recycling of catalyst Al₂O₃-b-0.05. Reaction conditions: 100 mg of glucose dissolved in 1000 mg of EMIMBr; 140 °C, 3 h; 50 mg of Al₂O₃-b-0.05 at the first run.

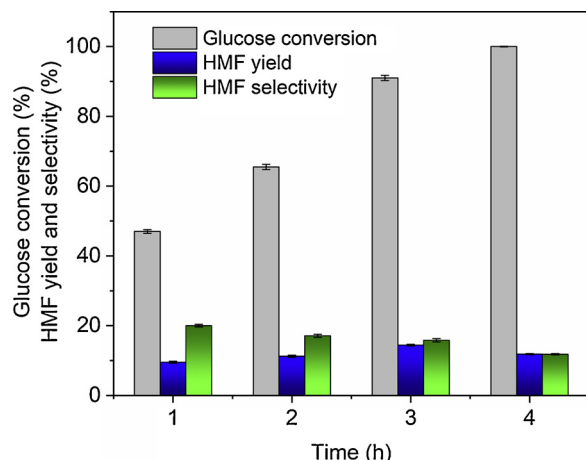


Fig. 9. Conversion of glucose into HMF in EMIMCl using Al₂O₃-b-0.05 as catalyst. Reaction conditions: 100 mg sugar dissolved in 1000 mg of EMIMCl; 50 mg of Al₂O₃-b-0.05; 140 °C.

Lower reaction temperature was not investigated because of the high melting point of EMIMBr (74.5 °C). The HMF yield in the EMIMBr/AlCl₃ system was much higher than that (1.6%) obtained with the EMIMCl/AlCl₃ system [47]. Although the initial glucose conversion rate and HMF formation rate in the homogeneous EMIMBr/AlCl₃ system at 80 °C were considerably higher than that obtained with the heterogeneous EMIMBr/Al₂O₃-b-0.05 system (Table 2), the maximal HMF yield of the former was obviously lower than the latter owing to the severe side-reactions in the EMIMBr/AlCl₃ system. Recently, it was observed that the acid Al₂O₃ exhibits better catalytic performance than natural and basic Al₂O₃ for the conversion of glucose to HMF in the water/MIBK system, but the HMF yield is less than 20% since the Al₂O₃ catalyst also accelerates the side-reactions [48]. These comparisons indicated that the EMIMBr/Al₂O₃-b-0.05 heterogeneous system is very efficient for the

conversion of glucose to HMF.

3.3. Reaction pathway for conversion of glucose to HMF

The low efficiency of glucose conversion to HMF in water and water-organic solvent biphasic reaction system are determined by the reaction pathway. As shown in Fig. 10a, the combination of Lewis acid and Brønsted acid is essential to achieve the one-pot conversion of glucose to HMF in these catalytic systems [49–52]. The isomerization of glucose to fructose, the rate-determining step, is a reversibly reaction catalyzed only by certain Lewis acid, base or enzyme with low efficiency [53]. The Brønsted acid used for fructose dehydration to HMF also catalyze decomposition of HMF to formic acid and levulinic acid as well as eventual condensation to humins. A balance between these reactions is especially difficult to achieve since the activation energy for fructose dehydration to HMF (29.4 kcal mol⁻¹) is obviously higher than that of HMF degradation to levulinic and formic acids (23.1 kcal mol⁻¹) [18]. Both glucose isomerization and fructose dehydration rate are limited at relative low reaction temperature, resulting in the inadequate reaction efficiency. Evaluating reaction temperature not only increases the fructose dehydration rate, but also accelerates the degradation of HMF and other intermediates, limiting the final HMF yields. The high HMF yields from these reaction systems are usually obtained at a very low initial glucose loading to control the side-reactions, which also hampers the process economics. Therefore, improving the intrinsic reaction efficiency of these catalytic systems is very challenging. The two-step glucose to HMF conversion processes also involve the isomerization of glucose to fructose, followed by dehydration of fructose to HMF [54]. The Brønsted acid catalyzed degradation of glucose and reaction intermediates to undesired products can be inhibited though this strategy since Brønsted acid is not added to the isomerization reaction system. However, the two-step processes still suffer from the inefficiency of glucose isomerization. Besides, the two-step processes need more separation and purification processes, inevitably increasing the energy consumption and process cost.

To improve the intrinsic HMF production efficiency, the design of novel reaction pathway with limited HMF degradation would be highly desirable. Several ionic liquid/metal chloride homogeneous reaction systems such as EMIMCl/CrCl₂, BMIMCl/CrCl₃ and EMIMBr/SnCl₄ enable the efficient and selective conversion of glucose to HMF under mild conditions, with reaction efficiencies obviously higher than the aforementioned water and water-organic solvent biphasic reaction systems [26,55]. As a proof of concept, we have shown that the EMIMBr/Al₂O₃-b-0.05 heterogeneous reaction system enables the efficient conversion of glucose to HMF while minimizing further degradation of the resulting HMF though a reaction pathway similar with the ionic liquid/metal chloride homogeneous reaction systems (Fig. 10b). Owing to the high Lewis acidity and low Brønsted acidity of Al₂O₃-b-0.05, the concentration of Brønsted acid in the EMIMBr/Al₂O₃-b-0.05 heterogeneous reaction system is low and the dehydration of fructose to HMF in the present reaction system is mainly catalyzed by EMIMBr, instead of Brønsted acid. As a consequence, the undesired side-reactions induced by Brønsted acid were remarkably inhibited in this reaction system. Moreover, since the ionic liquid catalyzed fructose dehydration rate exceeds glucose isomerization under most conditions, the rapid consumption of fructose could shift the reaction equilibrium and then

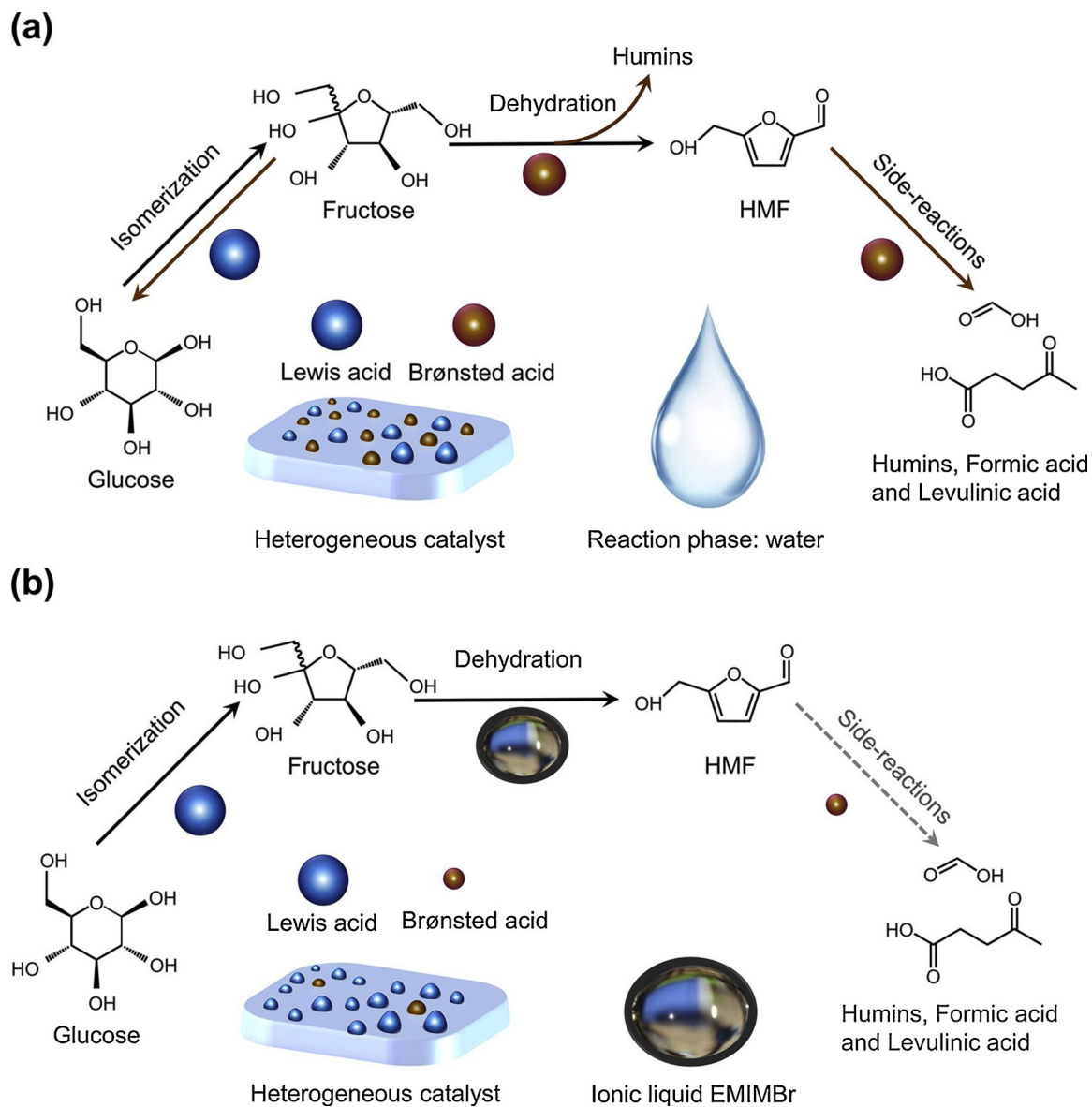


Fig. 10. Reaction pathway of glucose conversion in (a) the conventional reaction system and (b) the present reaction system.

promote the glucose isomerization. Besides, the strong Lewis acid which is indispensable for glucose isomerization is retained in Al_2O_3 -b-0.05. Therefore, the combined use of Al_2O_3 -b-0.05 and EMIMBr could increase the rate of glucose conversion to HMF more relative to degradation of the resulting HMF, thus improving the final HMF yield and selectivity. This strategy overcomes the longstanding limit on glucose loading for the conventional heterogeneous reaction systems and enables the efficient and selective production of HMF from high-concentration glucose. Compared with our previous work, the use of Al_2O_3 -b-0.05 to displace SnPO could reduce the cost of catalyst considerably [24]. Although the complete quench of the Brønsted acid in the heterogeneous catalyst is challenging, the elaborately regulation of the intensity and concentration of Lewis acid, may further improve the HMF yield and selectivity [27]. However, the practical application of the EMIMBr/ Al_2O_3 -b-0.05 system is still impractical because of the non-negligible cost of ionic liquid production and recovery. To solve this problem, the further screening of cheap ionic liquids and deep-eutectic solvents as well as the development of environmentally friendly and cheap solvent recycling process are of great importance.

4. Conclusion

A series of Al-containing materials were investigated as heterogeneous catalysts in ionic liquid EMIMBr to improve the HMF production efficiency. The detailed characterizations showed that Al_2O_3 -b-0.05 has high concentration of stable Lewis acid sites and low concentration of Brønsted acid sites, as is different from other Al-containing catalysts. The Al_2O_3 -b-0.05 exhibited higher catalytic activity than the other catalysts in the medium of EMIMBr, obtaining an HMF yield of 49.7% at the optimized condition. When EMIMCl was used as reaction medium, the HMF yield decreased to 14.4%. Moreover, the heterogeneous catalyst can be reused with same catalytic activity for at least three runs. As a proof of concept, this work demonstrated that the combined use of ionic liquids and heterogeneous catalyst with high Lewis acidity and low Brønsted acidity are effective strategy to improve the HMF production efficiency.

Acknowledgements

This work was supported by the National Natural Science Foundation of China (21878163), the China Postdoctoral Science

Foundation (2018M640231), the Fundamental Research Funds for the Central Universities, Natural Science Foundation of Tianjin, China (17JCZDJC39500), National Key Research Project (2018YFD080083-03), Science and Technology Demonstration Project of Industrial Integration and Development of Tianjin, China (17ZXYENC00100), National Natural Science Foundation of China (51708301), Natural Science Foundation of Tianjin, China (17JCZDJC39500), and Jinnan District Science and Technology Project of Tianjin, China (20171505).

Appendix A. Supplementary data

Supplementary material related to this article can be found, in the online version, at doi:<https://doi.org/10.1016/j.apcatb.2019.04.003>.

References

- Y.M. Questell-Santiago, R. Zambrano-Varela, M. Talebi Amiri, J.S. Luterbacher, Carbohydrate stabilization extends the kinetic limits of chemical polysaccharide depolymerization, *Nat. Chem.* 10 (2018) 1222–1228.
- X. Zhang, K. Wilson, A.F. Lee, Heterogeneously catalyzed hydrothermal processing of C₅–C₆ sugars, *Chem. Rev.* 116 (2016) 12328–12368.
- L. Jiang, L. Zhou, J. Chao, H. Zhao, T. Lu, Y. Su, X. Yang, J. Xu, Direct catalytic conversion of carbohydrates to methyl levulinate: synergy of solid Brønsted acid and Lewis acid, *Appl. Catal. B* 220 (2018) 589–596.
- S. Jia, X. He, J. Ma, K. Wang, Z. Xu, Z.C. Zhang, Efficient synthesis of 5-hydroxymethylfurfural from mannose with a reusable MCM-41-supported tin catalyst, *Catal. Sci. Technol.* 8 (2018) 5526–5534.
- Q. Hou, M. Ju, W. Li, L. Liu, Y. Chen, Q. Yang, Pretreatment of lignocellulosic biomass with ionic liquids and ionic liquid-based solvent systems, *Molecules* 22 (2017) 490.
- Q. Hou, W. Li, M. Ju, L. Liu, Y. Chen, Q. Yang, J. Wang, Separation of polysaccharides from rice husk and wheat bran using solvent system consisting of BMIMOAc and DMI, *Carbohydr. Polym.* 133 (2015) 517–523.
- F.J. Morales-Leal, J. Rivera de la Rosa, C.J. Lucio-Ortiz, D.A. De Haro-Del Rio, C. Solis Maldonado, S. Wi, L.B. Casabianca, C.D. Garcia, Dehydration of fructose over thiol- and sulfonic-modified alumina in a continuous reactor for 5-HMF production: study of catalyst stability by NMR, *Appl. Catal. B* 244 (2019) 250–261.
- K. Li, M. Du, P. Ji, Multifunctional tin-based heterogeneous catalyst for catalytic conversion of glucose to 5-Hydroxymethylfurfural, *ACS Sustain. Chem. Eng.* 6 (2018) 5636–5644.
- M.J. Kang, H. Park, J. Jegal, S.Y. Hwang, Y.S. Kang, H.G. Cha, Electrocatalysis of 5-hydroxymethylfurfural on cobalt based spinel catalysts with filamentous nanochitecture in alkaline media, *Appl. Catal. B* 242 (2019) 85–91.
- Z. Gao, C. Li, G. Fan, L. Yang, F. Li, Nitrogen-doped carbon-decorated copper catalyst for highly efficient transfer hydrogenolysis of 5-hydroxymethylfurfural to convertibly produce 2,5-dimethylfuran or 2,5-dimethyltetrahydrofuran, *Appl. Catal. B* 226 (2018) 523–533.
- I. Krivtsov, E.I. García-López, G. Marcà, L. Palmissano, Z. Amghouz, J.R. García, S. Ordóñez, E. Díaz, Selective photocatalytic oxidation of 5-hydroxymethyl-2-fural to 2,5-furaniccarboxaldehyde in aqueous suspension of g-C₃N₄, *Appl. Catal. B* 204 (2017) 430–439.
- H.-F. Ye, R. Shi, X. Yang, W.-F. Fu, Y. Chen, P-doped Zn_xCd_{1-x}S solid solutions as photocatalysts for hydrogen evolution from water splitting coupled with photocatalytic oxidation of 5-hydroxymethylfurfural, *Appl. Catal. B* 233 (2018) 70–79.
- Q. Sun, S. Wang, B. Aguilera, X. Meng, S. Ma, F.-S. Xiao, Creating solvation environments in heterogeneous catalysts for efficient biomass conversion, *Nat. Commun.* 9 (2018) 3236.
- T. Ji, Z. Li, C. Liu, X. Lu, L. Li, J. Zhu, Niobium-doped TiO₂ solid acid catalysts: strengthened interfacial polarization, amplified microwave heating and enhanced energy efficiency of hydroxymethylfurfural production, *Appl. Catal. B* 243 (2019) 741–749.
- T. Ji, R. Tu, L. Li, L. Mu, C. Liu, X. Lu, J. Zhu, Localizing microwave heat by surface polarization of titanate nanostructures for enhanced catalytic reaction efficiency, *Appl. Catal. B* 227 (2018) 266–275.
- K. Tsutsumi, N. Kurata, E. Takata, K. Furuchi, M. Nagano, K. Tabata, Silicon semiconductor-assisted Brønsted acid-catalyzed dehydration: highly selective synthesis of 5-hydroxymethylfurfural from fructose under visible light irradiation, *Appl. Catal. B* 147 (2014) 1009–1014.
- Q. Hou, W. Li, M. Ju, L. Liu, Y. Chen, Q. Yang, One-pot synthesis of sulfonated graphene oxide for efficient conversion of fructose into HMF, *RSC Adv.* 6 (2016) 104016–104024.
- K.R. Enslow, A.T. Bell, SnCl₄-catalyzed isomerization/dehydration of xylose and glucose to furanics in water, *Catal. Sci. Technol.* 5 (2015) 2839–2847.
- E. Nikolla, Y. Román-Leshkov, M. Moliner, M.E. Davis, “One-Pot” Synthesis of 5-(Hydroxymethyl)furfural from Carbohydrates using Tin-Beta Zeolite, *ACS Catal.* 1 (2011) 408–410.
- M.A. Mellmer, C. Sanpitakser, B. Demir, P. Bai, K. Ma, M. Neurock, J.A. Dumesic, Solvent-enabled control of reactivity for liquid-phase reactions of biomass-derived compounds, *Nat. Catal.* 1 (2018) 199–207.
- G. Tsilomelekitis, M.J. Orella, Z. Lin, Z. Cheng, W. Zheng, V. Nikolakis, D.G. Vlachos, Molecular structure, morphology and growth mechanisms and rates of 5-hydroxymethyl furfural (HMF) derived humins, *Green Chem.* 18 (2016) 1983–1993.
- J. Zhang, A. Das, R.S. Assary, L.A. Curtiss, E. Weitz, A combined experimental and computational study of the mechanism of fructose dehydration to 5-hydroxymethylfurfural in dimethylsulfoxide using Amberlyst 70, PO₄³⁻/niobic acid, or sulfuric acid catalysts, *Appl. Catal. B* 181 (2016) 874–887.
- Z. Cao, Z. Fan, Y. Chen, M. Li, T. Shen, C. Zhu, H. Ying, Efficient preparation of 5-hydroxymethylfurfural from cellulose in a biphasic system over hafnium phosphates, *Appl. Catal. B* 244 (2019) 170–177.
- Q. Hou, M. Zhen, L. Liu, Y. Chen, F. Huang, S. Zhang, W. Li, M. Ju, Tin phosphate as a heterogeneous catalyst for efficient dehydration of glucose into 5-hydroxymethylfurfural in ionic liquid, *Appl. Catal. B* 224 (2018) 183–193.
- H. Zhao, J.E. Holladay, H. Brown, Z.C. Zhang, Metal chlorides in ionic liquid solvents convert sugars to 5-Hydroxymethylfurfural, *Science* 316 (2007) 1597–1600.
- Q. Hou, W. Li, M. Zhen, L. Liu, Y. Chen, Q. Yang, F. Huang, S. Zhang, M. Ju, An ionic liquid-organic solvent biphasic system for efficient production of 5-hydroxymethylfurfural from carbohydrates at high concentrations, *RSC Adv.* 7 (2017) 47288–47296.
- M.A. Ardagh, Z. Bo, S.L. Nauert, J.M. Notestein, Depositing SiO₂ on Al₂O₃: a route to tunable Brønsted acid catalysts, *ACS Catal.* 6 (2016) 6156–6164.
- R. Estevez, S. Lopez-Pedrajas, D. Luna, F.M. Bautista, Microwave-assisted etherification of glycerol with tert-butyl alcohol over amorphous organosilica-aluminum phosphates, *Appl. Catal. B* 213 (2017) 42–52.
- I. Jiménez-Morales, M. Moreno-Recio, J. Santamaría-González, P. Maireles-Torres, A. Jiménez-López, Production of 5-hydroxymethylfurfural from glucose using aluminum doped MCM-41 silica as acid catalyst, *Appl. Catal. B* 164 (2015) 70–76.
- R. Locus, D. Verboekend, R. Zhong, K. Houthoofd, T. Jaumann, S. Oswald, L. Giebel, G. Baron, B.F. Sels, Enhanced acidity and accessibility in Al-MCM-41 through aluminum activation, *Chem. Mater.* 28 (2016) 7731–7743.
- F. Zeng, W.J. Tenn, S.N.V.K. Aki, J. Xu, B. Liu, K.L. Hohn, Influence of basicity on 1,3-butadiene formation from catalytic 2,3-butanediol dehydration over γ -alumina, *J. Catal.* 344 (2016) 77–89.
- R.M. Ravenelle, J.R. Copeland, W.-G. Kim, J.C. Crittenden, C. Sievers, Structural changes of γ -Al₂O₃-Supported catalysts in hot liquid water, *ACS Catal.* 1 (2011) 552–561.
- X. Song, P. Qu, H. Yang, X. He, G. Qiu, Synthesis of γ -Al₂O₃ nanoparticles by chemical precipitation method, *J. Cent. South Univ. Technol.* 12 (2005) 536–541.
- M. Auta, N.D. Amat Darbis, A.T. Mohd Din, B.H. Hameed, Fixed-bed column adsorption of carbon dioxide by sodium hydroxide modified activated alumina, *Chem. Eng. J.* 233 (2013) 80–87.
- V.V. Ordomsky, V.L. Sushkevich, J.C. Schouten, J. van der Schaaf, T.A. Nijhuis, Glucose dehydration to 5-hydroxymethylfurfural over phosphate catalysts, *J. Catal.* 300 (2013) 37–46.
- P.M. Bautista, J.M. Campelo, A. Garcia, D. Luna, J.M. Marinas, A.A. Romero, AlPO₄-Al₂O₃ catalysts with low alumina content: I. Structural and textural characterization of catalysts obtained with aqueous ammonia, *Appl. Catal. A* 96 (1993) 175–199.
- G.J. Hutchings, I.D. Hudson, D.G. Timms, Dehydration of 2-methylbutanal to isoprene using aluminium phosphate catalysts, *Catal. Lett.* 61 (1999) 219–224.
- J. Markovski, J. Garcia, K.D. Hristovski, P. Westerhoff, Nano-enabling of strong-base ion-exchange media via a room-temperature aluminum (hydr)oxide synthesis method to simultaneously remove nitrate and fluoride, *Sci. Total Environ.* 599–600 (2017) 1848–1855.
- R.E. Whitfield, Purification of Aqueous Hydrochloric Acid, US3411879A (1968).
- J.Z. Hu, S. Xu, J.H. Kwak, M.Y. Hu, C. Wan, Z. Zhao, J. Szanyi, X. Bao, X. Han, Y. Wang, C.H.F. Peden, High field ²⁷Al MAS NMR and TPD studies of active sites in ethanol dehydration using thermally treated transitional aluminas as catalysts, *J. Catal.* 336 (2016) 85–93.
- Z. Zhang, Y. Zhu, H. Asakura, B. Zhang, J. Zhang, M. Zhou, Y. Han, T. Tanaka, A. Wang, T. Zhang, N. Yan, Thermally stable single atom Pt/m-Al₂O₃ for selective hydrogenation and CO oxidation, *Nat. Commun.* 8 (2017) 16100.
- J.H. Kwak, J. Hu, D. Mei, C.-W. Yi, D.H. Kim, C.H.F. Peden, L.F. Allard, J. Szanyi, Coordinatively unsaturated Al³⁺ centers as binding sites for active catalyst phases of platinum on γ -Al₂O₃, *Science* 325 (2009) 1670–1673.
- J. Lee, E.J. Jang, J.H. Kwak, Acid-base properties of Al₂O₃: effects of morphology, crystalline phase, and additives, *J. Catal.* 345 (2017) 135–148.
- Y. Wang, G. Ding, X. Yang, H. Zheng, Y. Zhu, Y. Li, Selectively convert fructose to furfural or hydroxymethylfurfural on Beta zeolite: the manipulation of solvent effects, *Appl. Catal. B* 235 (2018) 150–157.
- G.S. Svenningsen, R. Kumar, C.E. Wyman, P. Christopher, Unifying mechanistic analysis of factors controlling selectivity in fructose dehydration to 5-hydroxymethylfurfural by homogeneous acid catalysts in aprotic solvents, *ACS Catal.* 8 (2018) 5591–5600.
- Y. Román-Leshkov, J.N. Chheda, J.A. Dumesic, Phase modifiers promote efficient production of hydroxymethylfurfural from fructose, *Science* 312 (2006) 1933–1937.
- D. Liu, E.Y.X. Chen, Ubiquitous aluminum alkyls and alkoxides as effective catalysts for glucose to HMF conversion in ionic liquids, *Appl. Catal. A* 435–436 (2012) 78–85.
- C. García-Sancho, I. Fúnez-Núñez, R. Moreno-Tost, J. Santamaría-González, E. Pérez-Inestrosa, J.L.G. Fierro, P. Maireles-Torres, Beneficial effects of calcium chloride on glucose dehydration to 5-hydroxymethylfurfural in the presence of alumina as catalyst, *Appl. Catal. B* 206 (2017) 617–625.
- Y.J. Pagán-Torres, T. Wang, J.M.R. Gallo, B.H. Shanks, J.A. Dumesic, Production of 5-Hydroxymethylfurfural from Glucose Using a Combination of Lewis and Brønsted Acid Catalysts in Water in a Biphasic Reactor with an Alkylphenol Solvent, *ACS*

Catal. 2 (2012) 930–934.

[50] P. Carniti, A. Gervasini, F. Bossola, V. Dal Santo, Cooperative action of Brønsted and Lewis acid sites of niobium phosphate catalysts for cellobiose conversion in water, *Appl. Catal. B* 193 (2016) 93–102.

[51] J. Guo, S. Zhu, Y. Cen, Z. Qin, J. Wang, W. Fan, Ordered mesoporous Nb-W oxides for the conversion of glucose to fructose, mannose and 5-hydroxymethylfurfural, *Appl. Catal. B* 200 (2017) 611–619.

[52] S. Campisi, S. Bennici, A. Auroux, P. Carniti, A. Gervasini, A rational revisiting of niobium oxophosphate catalysts for carbohydrate biomass reactions, *Top. Catal.* 61 (2018) 1939–1948.

[53] I. Graça, D. Iruretagoyena, D. Chadwick, Glucose isomerisation into fructose over magnesium-impregnated NaY zeolite catalysts, *Appl. Catal. B* 206 (2017) 434–443.

[54] T.L. Lohr, T.J. Marks, Orthogonal tandem catalysis, *Nat. Chem.* 7 (2015) 477.

[55] J. Zhou, Z. Xia, T. Huang, P. Yan, W. Xu, Z. Xu, J. Wang, Z.C. Zhang, An ionic liquid-organics-water ternary biphasic system enhances the 5-hydroxymethylfurfural yield in catalytic conversion of glucose at high concentrations, *Green Chem.* 17 (2015) 4206–4216.